Applied Thermal Engineering 51 (2013) 1055–1066

Contents lists available at SciVerse ScienceDirect

Applied Thermal Engineering

journal homepage: www.elsevier.com/locate/apthermeng

Thermal effect of lubricating oil in positive-displacement air compressors

Gianluca Valenti [a,*], Luigi Colombo [a], Stefano Murgia [b], Andrea Lucchini [a], Andrea Sampietro [a], Andrea Capoferri [b], Lucio Araneo [a]

[a] Politecnico di Milano – Dipartimento di Energia, Via R. Lambruschini 4, 20156 Milano, Italy
[b] Ing. Enea Mattei S.p.A., Strada Padana Superiore 307, 20090 Vimodrone (MI), Italy

HIGHLIGHTS

- Exploitation of thermal effect of oil in gas compressors is assessed numerically.
- Oil in 100 μm-diameter droplets mitigates effectively the gas temperature rise.
- Discharge temperature and compression work result to be much smaller than typical.
- An experimental setup is used to investigate oil atomization via commercial nozzles.
- A tested nozzle creates fine oil droplets and structures at conditions of interest.

ARTICLE INFO

Article history:
Received 24 May 2012
Accepted 12 October 2012
Available online 7 November 2012

Keywords:
Positive-displacement compressors
Oil spray
Heat transfer

ABSTRACT

The isentropic efficiency of positive-displacement compressors may be improved in order to follow an increasing demand for energy savings. This work analyzes the thermal effect of the lubricating oil presence in the air during compression with the scope of exploiting it as a thermal ballast to mitigate both the gas temperature rise and its compression work. The bibliographic review shows that other authors suggested that oil can have positive effects if properly injected. Here an energy balance analysis is executed with the scope of deriving relations for the gas–liquid compression in analogy with those typical for the gas-only compression and of confirming that ideally the liquid presence may have beneficial effects, making the gas–liquid compression even better than 1- and 2-time intercooled gas compressions. Given these positive results, a heat transfer analysis is conducted to model the thermal interaction between gas and oil droplets within a mid-size rotary vane air compressor. A droplet diameter of the order of 100 μm leads to large reductions of both temperature increase and compression work: air can exit the discharge port at a temperature as low as 60 °C and compression work can be lowered by 23–28% with respect to conventional compressors. Finally, a test rig is constructed and operated to investigate a large-flow and large-angle oil nozzle taken from the market showing that, at the operating conditions of a compressor, oil breaks up into small droplets and undefined structures with large exchange surfaces.

1. Introduction

Positive-displacement compressors have achieved high levels of reliability, a quality that has been so far the primary goal of their design. In recent years, however, the growing interest for energy savings in many industrial processes has favored an increasing attention also for high levels of performance. The present work originates from an industrial–academic collaboration focusing on the methods for enhancing oil-injected positive-displacement air compressors. At this first stage, the attention is placed on exploiting the thermal effect due to the presence of oil within the air. In conventional machines, oil is injected mainly to seal and lubricate the moving parts. It does not evaporate as it occurs in the so-called "wet compression" – an alternative that is being considered for gas turbines [1], refrigerators and heat pumps [2] – but it remains almost totally in the liquid form. If the oil is properly dispersed into the air, it is expected to function not only as a sealer and a lubricant but also as a thermal ballast.

The analysis of the energy balance of this "gas–liquid compression" is used here to study in general terms whether

* Corresponding author. Tel.: +39 (0)2 2399 3845.
E-mail address: gianluca.valenti@polimi.it (G. Valenti).
URL: http://www.gecos.polimi.it/

1359-4311/$ – see front matter © 2012 Elsevier Ltd. All rights reserved.
http://dx.doi.org/10.1016/j.applthermaleng.2012.10.040

a liquid in significant quantities within a gas can mitigate the gas temperature rise and, hence, its compression work. The subsequent analysis of the heat transfer verifies specifically for oil-injected air compressors how small the droplets must be to allow an appreciable energy transfer from the air to the oil. Finally, an experimental investigation is employed to provide preliminary indications on whether a selected commercial oil nozzle can generate the desired sprays.

2. Bibliographic review

The oil injection in positive-displacement compressors, especially in screw compressors as it will be shown, has been investigated by a number of authors in last decades. In 1986 Singh and Bowman [3] developed a mathematical model to study the heat transfer phenomenon between gas and oil in a screw compressor and to predict the compressor performance under diverse working conditions. The authors underline that substituting a "polytropic" compression with an isothermal one may yield a decrease of 15–20% in the specific work. In their analysis the oil droplets are assumed to be: spherical, non-deformable, non-evaporating, scattered distributed, and non-interacting; moreover, the heat transfer is assumed to take place only during the droplets free-flight time, that is before they impact onto the surrounding walls. The authors conclude that a droplet diameter of 1000 μm leads to a 7% reduction of the specific work whereas a droplet diameter of 100 μm to 8.3% reduction. They state that these results are in agreement with experimental data that, unfortunately, are not reported. Furthermore, they add that the oil injection position is as important as the nozzle and that a pump is not required to atomize the oil.

Similarly, Stosic et al. (1988) [4] analyzed the oil injection in a screw compressor by mean of a numerical model based on the internal energy conservation equation, the continuity equation, the equation of state for the gas, and the Ranz–Marshall correlation (recalled in Section 3.2). The investigated parameters are: droplets diameter, injection position, oil inlet temperature, oil-to-gas mass ratio, and oil viscosity. The authors conclude that the oil temperature follows the gas temperature closely exception made for droplet sizes greater than 1 mm and that the oil temperature and injection location affect significantly the performance; conversely, the mass ratio and the oil viscosity have a small influence. Four years later the same authors [5] built a test rig employed to compare a standard compressor against a compressor with an optimized oil injection system. With the new configuration the oil-to-gas mass ratio is reduced by 2–3% and the power consumption by 2.8–7.4% maintaining the same delivery conditions.

Fujiwara and Osada (1995) [6] developed a numerical model, similar to the previous ones, and built a test rig in order to simulate the working process of a screw compressor and to verify new rotor profiles characterized by higher performances. The authors estimate a flow coefficient, that they employ to model the screw leakages, and the heat transfer coefficient from experimental data. An innovative rotor profile is manufactured, tested and applied to a commercial series of air screw compressors: in the rotor speed range from 2000 to 6000 rpm, volumetric and adiabatic efficiencies are constantly a few percent points higher than those of the conventional profile and they can exceed 90% at higher speeds.

As all the previous authors, De Paepe et al. [7] investigated in 2004 screw compressor by implementing a thermodynamic model and building a test rig. The compression is modeled as a polytropic transformation while the heat exchange is evaluated by the mean of a cooling effectiveness estimated experimentally. According to the author, the oil atomization does not affect appreciably the compressor performance. In particular, raising the oil flow rate by 10%, lowers the specific work by 0.2%; lowering the oil injection temperature by 5 °C, lowers the specific work by 0.5%; raising the cooling effectiveness by 10 points, lowers the specific work by 0.05%. Finally, the injection location has a very little influence.

In 2007 Seshaiah et al. [8] developed a mathematical model and built a test rig for an oil injected twin screw compressor. The model is based on the ideal gas law and standard thermodynamic relations, whereas the heat transfer coefficient is obtained experimentally in the same manner as Fujiwara and Osada [6]. The study aims at investigating the influence of various operating and design parameters on the compressor performance, focusing primarily on the compression of air and helium. The authors conclude that most of the heat transfer takes place after the gas and the oil leave the twin screw. Three years later the same authors [9] studied, both numerically and experimentally, the compression process of nitrogen, argon, helium, and air. Additional analysis on the effects of oil injection parameters such as oil inlet temperature and oil injection rate are conducted. For all cases both the adiabatic and the volumetric efficiencies increase when lowering the oil injection temperature for a wide range of oil injection rates. In particular, lowering the oil inlet temperature is more effective than injecting a higher quantity.

Oil atomization in conventional rotary vane compressors has been explored by Cipollone et al. [10] in recent years from both numerical and experimental perspectives. The numerical results are validated measuring the pressure evolution inside the compressor vanes. This study appears to be the first successful realization of the direct measuring of pressure inside the vane during compression. The authors conclude that the compression is adiabatic and, consequently, the heat transfer between gas and oil is negligible.

In summary, the oil injection within positive-displacement compressors has been investigated in the past, focusing almost exclusively on screw compressors, and has been proved by most studies to have positive effects on the compressor performance if properly executed.

3. Theoretical analyses

The thermal effect of lubricating oil in positive-displacement air compressors is investigated theoretically by mean of an energy balance analysis and a heat transfer analysis. The assumptions common to both analyses are listed and commented in the following.

- The gas behaves as an ideal gas having a constant isobaric specific heat.
- The liquid behaves as an incompressible fluid having a constant specific heat.
- The gas is non-soluble into the liquid.
- The liquid is non-volatile into the gas.
- The compression is adiabatic toward the surroundings.

The assumptions of ideality of gas and liquid are common for oil-injected air compressors, as proved by the bibliographic review, because temperatures are, on one side, much higher that oxygen and nitrogen critical temperatures and, on the other, much lower than oil critical temperature; in addition, variations of temperature as well as of pressure are small. The gas is considered non-soluble into the liquid, or at least not in large quantities, based on industrial experience and the liquid is non-volatile because it has a very low saturation pressure. As a consequence of the non-solubility and the non-volatility, exclusively the thermal interaction between gas and liquid is considered. The general parameters are given in Table 1.

Table 1
General parameters for both the energy balance and the heat transfer analyses.

Parameter	Symbol	Unit	Value
Gas			
Name			Air
Molar mass	M^g	kg kmol^{-1}	28.96
Isobaric specific heat	c_p^g	J kg^{-1} K^{-1}	1007
Liquid			
Name			Lube oil
Density	ρ^l	kg m^{-3}	959
Isobaric specific heat	c^l	J kg^{-1} K^{-1}	2800
Compression			
Initial temperature	T_i^g and T_i^l	°C	15
Inlet pressure	P_i	bar	1.00
Outlet pressure	P_f	bar	9.40

3.1. Energy balance analysis

In this section the equations for the energy balance of the gas–liquid compression are manipulated in analogy with those for the gas-only compression that appear in textbooks. In addition, a novel method to evaluate the isentropic efficiency of the gas–liquid compression is proposed. On top of the assumptions mentioned at the beginning of Section 3, this analysis hypothesizes that gas and oil have the same temperature at the suction and at the discharge ports of the compressor. Nevertheless, they may be diverse during the compression itself, leading to entropy generation due to the temperature difference.

The subscripts i and f indicate an initial state and a final state of a property. Recalling that the process is adiabatic and neglecting the gravimetric and kinetic term differences, the overall compression power (or shaft power) $\dot{L}$ [W], taken positive if transferred into the gas–liquid system from the surrounding, is computed from the steady-state energy balance applied from the suction to the discharge ports of the compressor:

$$\dot{L} = \dot{m}\left(h_f - h_i\right) \tag{1}$$

where $\dot{m}$ [kg s^{-1}]and h [J kg^{-1}] are the mass flow and the mass-specific enthalpy of the gas–liquid mixture. Similarly, the rate of entropy generation $\dot{S}_{irr}$ [W K^{-1}] due to irreversibility is:

$$\dot{S}_{irr} = \dot{m}\left(s_f - s_i\right) \tag{2}$$

where s [J kg^{-1} K^{-1}] is the mass-specific entropy of the gas–liquid mixture flow.

Given the non-volatility and the non-solubility assumptions, both the mass-specific enthalpy and entropy of a gas–liquid flow are computed as weighted averages of the pure gas and the pure liquid properties, where the weights are the mass fractions. As a consequence, equations (1) and (2) can be written as sums of pure gas and pure liquid extensive properties:

$$\dot{L} = \dot{m}^g c_p^g\left(T_f - T_i\right) + \dot{m}^l\left[c^l\left(T_f - T_i\right) + \frac{P_f - P_i}{\rho^l}\right] \tag{3}$$

and:

$$\dot{S}_{irr} = \dot{m}^g\left(c_p^g \ln\frac{T_f}{T_i} - R\ln\frac{P_f}{P_i}\right) + \dot{m}^l c^l \ln\frac{T_f}{T_i} \tag{4}$$

where g and l refer to gas and liquid, c is the mass-specific heat [J kg^{-1} K^{-1}] (c_p is in particular the mass-specific heat at constant pressure) and R is the gas constant [J kg^{-1} K^{-1}]. These two relations can be rearranged as:

$$\dot{L} = \dot{m}^g\left[\hat{c}\left(T_f - T_i\right) + \varepsilon_m\frac{P_f - P_i}{\rho^l}\right] \tag{5}$$

and:

$$\dot{S}_{irr} = \dot{m}^g\left(\hat{c}\ln\frac{T_f}{T_i} - R\ln\frac{P_f}{P_i}\right) \tag{6}$$

The modified specific heat, $\hat{c}$ [J kg^{-1} K^{-1}], that appears in the previous equations is defined as:

$$\hat{c} \stackrel{\text{def}}{=} c_p^g(1 + \varepsilon_m\varepsilon_c) \tag{7}$$

where the liquid-to-gas mass ratio, ε_m [−], is:

$$\varepsilon_m \stackrel{\text{def}}{=} \frac{\dot{m}^l}{\dot{m}^g} \tag{8}$$

and the liquid-to-gas heat ratio ε_c [−]:

$$\varepsilon_c \stackrel{\text{def}}{=} \frac{c^l}{c_p^g} \tag{9}$$

Being the process adiabatic, if it is ideal (reversible) it is also isentropic. Substituting the condition $\dot{S}_{irr} = 0$ into equation (6) yields:

$$\frac{T_{fs}}{T_i} = \left(\frac{P_f}{P_i}\right)^{\widehat{\Theta}} \tag{10}$$

where T_{fs} indicates the isentropic (ideal) final temperature. The modified theta parameter, $\widehat{\Theta}$ [−], that appears in the previous equation is defined as:

$$\widehat{\Theta} \stackrel{\text{def}}{=} \frac{R}{\hat{c}} \tag{11}$$

Equations (10) and (11) become the well-known gas-only relations for ε_m equal to zero. The ideal overall compression power turns to be:

$$\dot{L}_{id} = \dot{m}^g\left[\hat{c}T_i\left(\beta^{\widehat{\Theta}} - 1\right) + \varepsilon_m\frac{P_i(\beta - 1)}{\rho^l}\right] \tag{12}$$

The isentropic efficiency for a compression process is by definition:

$$\eta_s \stackrel{\text{def}}{=} \frac{\dot{L}_{id}}{\dot{L}} \tag{13}$$

where $\dot{L}_{id}$ shall be calculated accordingly to equation (12). In contrast, the efficiency of oil-injected positive-displacement compressors is often calculated ignoring the liquid presence and, thus, adopting:

$$\dot{L}_{id} = \dot{m}^g c_p^g T_i\left(\beta^{\Theta} - 1\right), \quad \text{if } \varepsilon_m = 0 \tag{14}$$

3.1.1. Parametric investigations

The temperature increase as well as the overall compression power of the gas–liquid (adiabatic) compression are compared against those of the gas-only isothermal compression and j-time intercooled compressions. The gas-only compression is taken as reference. For simplicity, all compressions are assumed to be ideal.

Mathematically, τ indicates the ratio of the temperature increase of an ideal compression with respect to the ideal gas-only compression, while λ the ratio of the ideal compression works. Schematically:

$$\tau \stackrel{\text{def}}{=} \frac{T_{\text{fs}} - T_{\text{i}} \text{ for any compression}}{T_{\text{fs}} - T_{\text{i}} \text{ for gas-only compression}} \tag{15}$$

and:

$$\lambda \stackrel{\text{def}}{=} \frac{\dot{L}_{\text{id}} \text{ for any compression}}{\dot{L}_{\text{id}} \text{ for gas-only compression}} \tag{16}$$

The resulting relations of τ and λ are reported in Table 2. These relations are applied to the demonstrative case of air compression, adopting the parameters from Table 1, in order to identify if gas–liquid compression may be competitive, at least under ideality.

3.2. Heat transfer analysis

The heat transfer between gas and liquid during compression is investigated in this section. During the process the two phases are generally not in thermal equilibrium and, hence, heat transfer takes place. The heat transfer rate depends on several factors: the area of the liquid–gas interface, the heat transfer coefficients between the phases and the temperature difference itself. Furthermore, the same liquid-to-gas mass ratio ε_{m} can be obtained with different patterns of the mixture: for instance, oil can be injected as a continuous phase or as a dispersed one. Thus, it is important to assess the conditions under which the results of the energy balance analysis can be technically approached. As an initial step, in order to identify the main parameters and their relative influence, the heat transfer between liquid and gas is described under certain simplifying assumptions on top of the general assumption described at the beginning of Section 3. These additional assumptions are here reported.

- The liquid phase is dispersed within the gas in form of droplets, which is the usual flow pattern in wet compression systems [1,2] and in all the reviewed studies [3–10].
- Droplets are non-deformable spheres of equal radius, despite injectors provide a range of diameters with a most probable value as explained by Lefebvre [11].
- The droplet temperature is uniform, given that the following condition on the Biot number of the droplet Bi [−] is satisfied [12]:

$$\text{Bi} \stackrel{\text{def}}{=} \frac{\alpha D}{6k^{\text{l}}} \leq 0.1 \tag{17}$$

- where α is the convective heat transfer coefficient at the droplet surface [W m^{-2} K^{-1}], D is the droplet diameter [m] and k^{l} is the liquid thermal conductivity [W m^{-1} K^{-1}].
- The gas phase is well mixed, because it is expected that the compression occurs uniformly within the chamber, where the term “chamber” refers to the gas–liquid closed system confined by the compressor parts (in a rotary vane compressor: rotor, stator and two adjacent vanes).
- The heat transfer between a droplet and the gas is driven by convection and the convective heat transfer coefficient can be evaluated from the Nusselt number, Nu_{D} [−], defined as:

$$Nu_{\text{D}} \stackrel{\text{def}}{=} \frac{\alpha D}{k^{\text{g}}} \tag{18}$$

- where k^{g} is the gas thermal conductivity [W m^{-1} K^{-1}]. The Nusselt number may be estimated by suitable correlations developed for droplets. In particular, if the two phases are in relative motion, the Ranz–Marshall correlation can be used [13]:

$$\text{Nu}_{\text{D}} = 2 + 0.6\text{Re}_{\text{D}}^{0.5}\text{Pr}^{1/3} \tag{19}$$

- where the relative velocity appears in the Reynolds number, Re_{D} [−]. On the other hand, if droplets are suspended in the gas phase with no relative motion, the Churchill correlation can be used [14]:

$$\text{Nu}_{\text{D}} = 2 + \frac{0.589\text{Ra}_{\text{D}}^{1/4}}{\left[1 + (0.469/\text{Pr})^{9/16}\right]^{4/9}} \tag{20}$$

- where Ra_{D} is the Rayleigh number [−]. For both the situations, the worst case corresponding to pure conduction is characterized by Nu_{D} equal to 2, which will be adopted in most cases later analyzed.
- Marangoni convection within the droplet is neglected.

The instantaneous energy balance applied to a single compression chamber, which is a closed system opposed to the open system of the energy balance analysis, is:

$$\frac{\text{d}U^{\text{l}}}{\text{d}t} + \frac{\text{d}U^{\text{g}}}{\text{d}t} = \dot{L}^{\text{g}} \tag{21}$$

where U is the internal energy [J] and $\dot{L}^{\text{g}}$ is the mechanical power [W] required for the compression of the gas contained in the chamber itself, taken positive if transferred into the gas from the surroundings. Furthermore:

$$\frac{\text{d}U^{\text{g}}}{\text{d}t} = m^{\text{g}} c_{\text{v}}^{\text{g}} \frac{\text{d}T^{\text{g}}}{\text{d}t} \tag{22}$$

and:

$$\frac{dU^{l}}{dt} = m^{l} c^{l} \frac{dT^{l}}{dt} = \alpha A\left(T^{g} - T^{l}\right) \tag{23}$$

where m [kg] and A [m^2] denote the mass (of the gas or the liquid) and the heat transfer surface of all droplets, and c_{v}^{g} the mass-specific heat at constant volume (related to that at constant pressure by the Mayer relation $c_{\text{p}}^{\text{g}} = c_{\text{v}}^{\text{g}} + R$). The surface A is given by the product of the number N of droplets and the surface of a single (spherical) droplet:

Table 2
Relations for the ratios of the temperature increase, τ, and compression work, λ, of the gas–liquid compression, the (gas-only) isothermal compression, (gas-only) j-time intercooled compressions taking as reference the gas-only (adiabatic) compression. All processes are ideal.

Ideal compression type	τ [−]	λ [−]
Gas–liquid	$\frac{\beta^{\widehat{\Theta}} - 1}{\beta^{\widehat{\Theta}} - 1}$	$\frac{\widehat{c}T_{\text{i}}(\beta^{\widehat{\Theta}} - 1) + \varepsilon_{\text{m}}\frac{P_{\text{i}}(\beta - 1)}{\rho^{\text{l}}}}{c_{\text{p}}^{\text{g}}T_{\text{i}}(\beta^{\Theta} - 1)}$
(Gas-only) isothermal	0	$\frac{R_{\text{g}} \ln \beta}{c_{\text{p}}^{\text{g}}T_{\text{i}}(\beta^{\Theta} - 1)}$
(Gas-only) j-time intercooled	$\frac{\beta^{\frac{\Theta}{j+1}} - 1}{\beta^{\Theta} - 1}$	$\frac{(j+1)c_{\text{p}}^{\text{g}}\left(\beta^{\frac{\Theta}{j+1}} - 1\right)}{c_{\text{p}}^{\text{g}}(\beta^{\Theta} - 1)}$

$$A = N\pi D^2 \tag{24}$$

where the number of droplets is given by the division of the mass of the liquid and the mass of a single (spherical) droplet:

$$N = \frac{m^{\mathrm{l}}}{\rho^{\mathrm{l}}\frac{\pi}{6}D^3} \tag{25}$$

The chamber compression power is determined by:

$$\dot{L}^{\mathrm{g}} = -P\frac{\mathrm{d}V^{\mathrm{g}}}{\mathrm{d}t} \tag{26}$$

The chamber volume is known geometrically as a function of the chamber angle, ϑ [deg], that is $V(\vartheta)$. The chamber angle (or simply angle) of a rotary vane compressor is the angular position of the trailing vane with respect to the tangent point between rotor and stator. Therefore, the time variation of the chamber volume is expressed through the time variation of the chamber angle, $V(\vartheta(t))$, that is related to the rotational speed of the shaft, Ω [rpm], via:

$$\vartheta = \frac{\pi}{30}\Omega t \tag{27}$$

Because the liquid phase is incompressible, the gas volume is determined as:

$$V^{g}(t) = V(t) - V^{l} \tag{28}$$

On the other hand, pressure is related to volume and temperature by the ideal gas law:

$$PV^{\mathrm{g}} = m^{\mathrm{g}}RT^{\mathrm{g}} \tag{29}$$

The system of these relations, equations (21)–(29), allows to calculate the variation of the gas and liquid temperature during the compression. The solution is obtained numerically by adopting the backward Euler method [15] and implementing the model in a computer software.

Finally, the overall compression power (or shaft power), $\dot{L}$ which refers to the open system, is obtained by combining the chamber compression power, $\dot{L}^{\mathrm{g}}$ which refers instead to the closed system, with the flow power of the gas–liquid mixture at the suction and the discharge ports. Mathematically:

$$\dot{L} = \dot{L}^{\mathrm{g}} + P_{\mathrm{f}}\dot{V}_{\mathrm{f}} - P_{\mathrm{i}}\dot{V}_{\mathrm{i}} \tag{30}$$

Compression powers can be expressed in terms specific to the mass of gas, m^{g}, as:

$$l^{\mathrm{g}} = \frac{\dot{L}^{\mathrm{g}}}{\dot{m}^{\mathrm{g}}} \tag{31}$$

and:

$$l = \frac{\dot{L}}{\dot{m}^{\mathrm{g}}} \tag{32}$$

Finally, at each time step the gas mass-specific heat along the compression process, $c_{\mathrm{x}}^{\mathrm{g}}$ [J kg^{-1} K^{-1}], can be evaluated as:

$$c_{\mathrm{x}}^{\mathrm{g}} = \frac{1}{m^{\mathrm{g}}}\left(\frac{\mathrm{d}Q}{\mathrm{d}T}\right)_{\mathrm{x}} \tag{33}$$

where dQ [J] is the heat between the gas and the liquid. For comparison with a polytropic compression of an ideal gas, an equivalent compression index n [−] can be defined as:

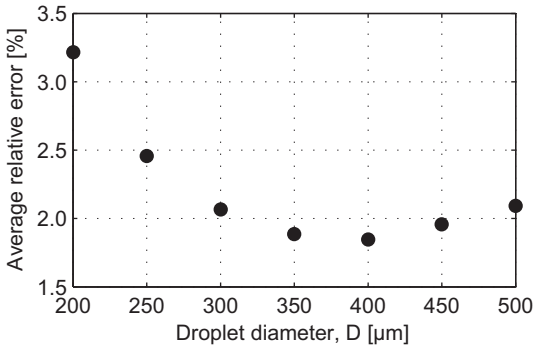

Fig. 1. Average relative error [%] as a function of the droplet diameter D [μm] computed for the validation of the heat transfer model.

$$n = \frac{c_{\mathrm{x}} - c_{\mathrm{p}}}{c_{\mathrm{x}} - c_{\mathrm{v}}} \tag{34}$$

3.2.1. Validation

The numerical model is validated with the experimental data collected by Cipollone et al. [10] on a mid-size rotary vane compressor equipped with a standard oil injection system. The validation is conducted comparing the pressure values inside the chamber during the whole process. It is assumed that heat transfer occurs by pure conduction, that is Nusselt number $\mathrm{Nu_D}$ equal to 2, which is the most conservative scenario. The droplet diameter D is varied in a discrete manner until it is reached the minimum value of the average relative error [%] between the measured and the calculated pressures. Fig. 1 shows that the minimum of 1.85% is reached for a diameter of 400 μm. The pressure variation during the process as a function of the chamber position is illustrated by Fig. 2, in which the solid line represents the calculated pressure, the dashed line the measured one, and the dots the relative error. The relative error never exceeds 4%, yielding a satisfactory validation. As explained by Cipollone et al. [10], the discontinuities of the relative error line are due to the fact that the experimental series is built from union of the measurements of different pressure transducers that are fixed on the case and, thus, do not rotate with the chamber.

3.2.2. Case studies

The heat transfer model is employed to analyze the mid-size commercial compressor adopted for the validation through seven

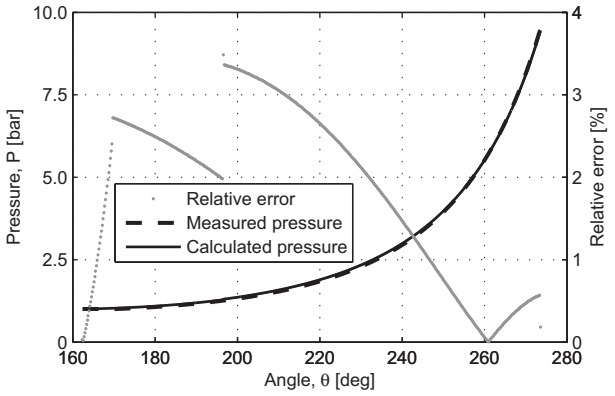

Fig. 2. Pressure variation during compression as a function of the chamber position (the solid line represents the calculated pressure, the dashed line the measured one, and the dots the relative error). Discontinuities of the relative error line are due to the fact that the experimental series is built from the measurement of different pressure transducers fixed on the compressor case.

Table 3
Additional parameters for the heat transfer analysis of air compression.

Parameter	Symbol	Unit	Value
Gas			
Thermal conductivity	k^g	W m^{-1} K^{-1}	0.028
Liquid			
Thermal conductivity	k^l	W m^{-1} K^{-1}	0.128
Compression			
Shaft rotational speed	Ω	rpm	1500

case studies. These cases are defined varying the following parameters:

- inlet air temperature (equal to either 50 °C or 15 °C),
- inlet oil temperature (80 °C or 25 °C),
- droplet diameter (400 μm or 100 μm),
- liquid-to-gas mass ratio (10 or the optimal value that minimizes the mass-specific compression work or even 0 to replicate the gas-only compression),
- Nusselt number (2 or 6 as explained below).

The working conditions of the validation are taken for the first case. Then each parameter is set, one at a time, to its best attainable value. All other parameters, including suction and discharge pressures and the geometrical dimensions but the discharge port location, are kept constant and equal to the values reported in Tables 1 and 3. The discharge port is moved angularly to achieve the targeted discharge pressure. For comparison, a last case of gas-only compression is included. The cases are described below and summarized in Table 4.

Case 1. It employs the same working conditions of the validation study: inlet air temperature of 50 °C, inlet oil temperature 80 °C, droplet diameter 400 μm, liquid-to-gas mass ratio 10, Nusselt number 2. In particular, air inlet temperature is relatively high due to the experimental setup design utilized by Cipollone et al. [10]; moreover, inlet oil temperature is also high in order to avoid the condensation of the water present in the air.
Case 2. The inlet air temperature is lowered to 15 °C, which is representative of the Italian average outdoor temperature. It implies that the fresh air entering the compressor is not heated by the setup parts and instrumentations as in Case 1.
Case 3. The inlet oil temperature is lowered to 25 °C, assuming that oil is cooled by an air-cooler characterized by a minimum temperature difference of 10 °C, which is technically achievable, and that the water condensation issue is solved by other than thermal means.
Case 4. The droplet diameter is lowered to 100 μm, according to the general performance of commercial oil nozzles partly confirmed by the experimental indications illustrated in Section 5.
Case 5. The liquid-to-gas mass ratio is increased to 16, which is the value that minimizes the mass-specific overall compression work as explained in Section 4 and visualized by Fig. 5.
Case 6. The Nusselt number is increased to 6 (see below) and the liquid-to-gas mass ratio is set to the optimal value of 12 (Section 4 and Fig. 5).
Case 7. The liquid-to-gas mass ratio is set to 0 in order to simulate the gas-only compression.

A figure for the maximum value of the Nusselt number is estimated considering that gas–liquid convection may be driven by a relative velocity of 10 m s^{-1}, which is the typical vane velocity at the tip for a mid-size compressor and it is also a representative value for the oil injection velocity (as explained in Section 5). This velocity yields a Reynolds number Re_D equal to 62.5 for a droplet of 100 μm considering a kinematic viscosity of air of 1.6×10^{-5} m^2 s^{-1}. Thus, the Nusselt number calculated by way of equation (19) is roughly 6, the value adopted in Case 6, employing a Prandtl number of air of 0.71. This value of the Nusselt number yields a Biot number equal to 0.2 for the sole Case 6, which does not respect equation (17), but it is still considered acceptable for the purposes of this work.

4. Results and discussion

The results of the parametric investigations of the energy balance analysis are reported graphically in Fig. 3. The temperature increase of the gas–liquid compression is lower than 1- and 2-time intercooled compressions for a liquid-to-gas mass ratio ε_m greater than 1. Moreover, it is much lower than the case of gas-only compression for a wide range of values of the mass ratio. Therefore, the liquid is ideally an effective thermal ballast that allows to reduce the temperature increase of the gas phase during compression and to generate potentially a compressed yet cold gas.

From a standpoint of the ideal compression work, the gas–liquid compression is not competitive with respect to the intercooled compression for low quantities of liquid, that is ε_m smaller than 0.5, because the heat capacity of the liquid is too small. The gas–liquid compression is also not competitive for high quantities of liquid, that is ε_m greater than 30, because the parasitic energy requirement for compressing the liquid outsets the positive effect of a very large heat capacity of the liquid itself. However, the gas–liquid compression is ideally better than the 2-time intercooled compression for intermediate mass ratios between 2 and 20 and approaches the isothermal compression for a mass ratio of about 5. For reference, existing positive-displacement compressors typically operate with liquid-to-gas mass ratios from 1 to 10.

The computed parameters for the case studies of the heat transfer analysis are visualized in Fig. 4. Cases with the larger

Table 4
Parameters of the case studies investigated in the heat transfer analysis.

Parameter	Symbol	Units	Case 1	Case 2	Case 3	Case 4	Case 5	Case 6	Case 7
Inlet air temperature	T_i^g	°C	50	15	15	15	15	15	15
Inlet oil temperature	T_i^l	°C	80	80	25	25	25	25	–
Droplet diameter	D	μm	400	400	400	100	100	100	–
Liquid-to-gas mass ratio	ε_m	–	10	10	10	10	16[a]	12[a]	0
Nusselt number	Nu_D	–	2	2	2	2	2	6	–

[a] Optimal value that minimizes the mass-specific compression power (see Fig. 5).

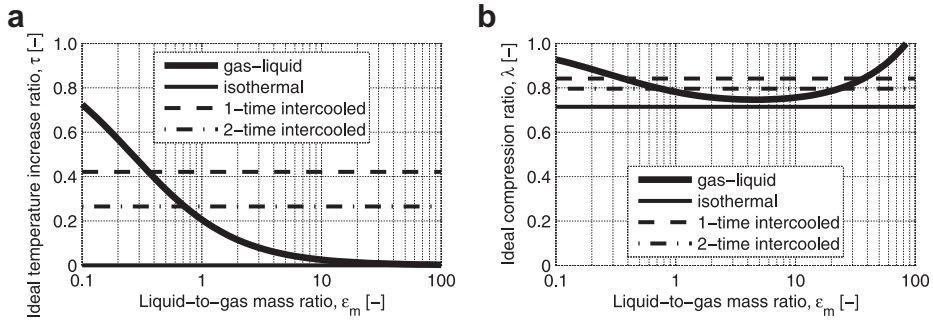

Fig. 3. Ratios of the temperature increase, τ, and compression work, λ, of the gas–liquid compression, the (gas-only) isothermal compression, (gas-only) 1- and 2-time intercooled compressions taking as reference the gas-only (adiabatic) compression, which is represented by τ and λ equal to unity. All processes are ideal.

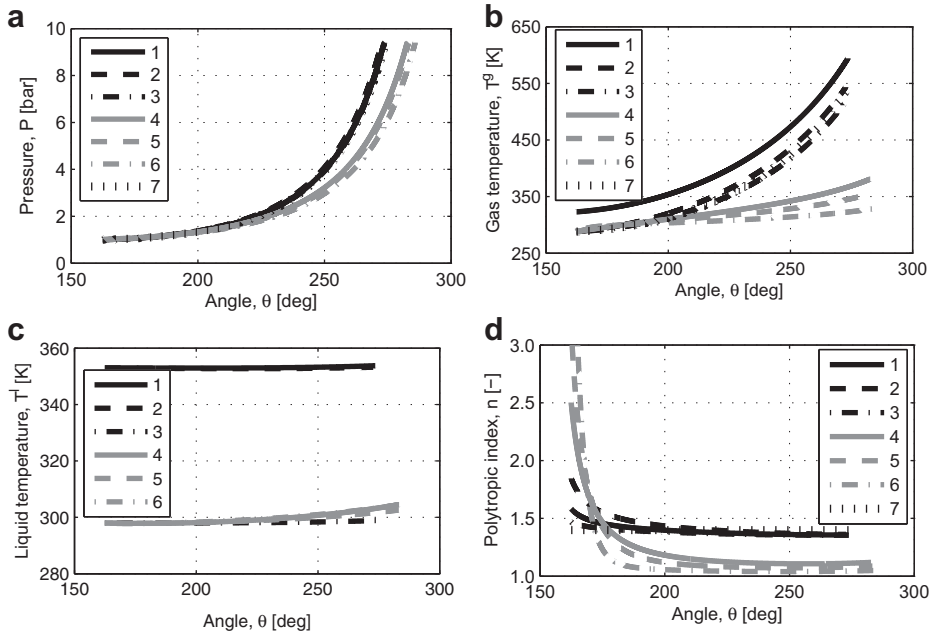

Fig. 4. Calculated properties for the case studies of the heat transfer analysis as a function of the chamber angle, ϑ [deg], from the suction to the discharge port; from top-left in clockwise order: pressure, P [bar], gas and oil temperature, T^g and T^l [K] and equivalent compression index, n [–].

droplet diameter (1–3 and 7) are indicated by black lines (continuous, dash and dot-and-dash), whereas those with the smaller diameter (4–6) with gray lines. The case of gas-only compression is indicated by a black dot line. The cases with larger or no droplets

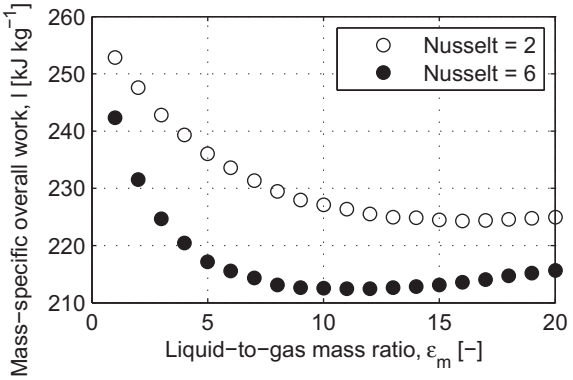

Fig. 5. Mass-specific overall compression work, $l^{\leftarrow}$ [kJ kg^{-1}], as a function of the liquid-to-gas mass ratio, ε_m [–], employed for determining optimal ratios: the resulting values are 16 for Case 5 and 12 for Case 6.

are characterized by steeper pressure increase because of the strong influence of the gas heating on pressure itself. This is a clear sign that oil is not interacting thermally. In contrast, cases with smaller droplets have a softer pressure increase and, thus, require a longer rotation to reach the targeted pressure, the longest being Case 6. This is a clear sign instead that the oil is interacting. These concepts are confirmed by the gas and the liquid temperature trends: black lines achieve much higher gas temperatures than the gray lines. In particular, a colder gas at the inlet leads necessarily to a colder gas at the outlet. In addition, a hot oil at the inlet can lead to a gas hotter than the case of gas-only compression: Case 2 outlet gas temperature is slightly higher than Case 7 because a moderate heat exchange is occurring. On the other hand, Cases 5 and 6 generate a compressed gas as cold as 330 K (about 60 °C). Interestingly, even in those cases in which oil is acting thermally (4–6), the liquid temperature increase is very modest due to its very large thermal capacity; all other cases are almost flat. The polytropic index of a compression gives information on the type of the process: the closer the value to the heat capacity ratio (that is the ratio of the heat capacity at constant pressure and that at constant volume, equal to 1.4 for air) the closer the process to an adiabatic compression; the closer instead to unity, the closer to an isothermal

Table 5
Results of the case studies investigated in the heat transfer analysis.

Parameter	Symbol	Units	Case 1	Case 2	Case 3	Case 4	Case 5	Case 6	Case 7
Mass-specific overall work[a,b]	l	kJ kg^{-1}	296.4	270.5	263.3	227.1	224.6	212.5	258.9
Isentropic efficiency[c]	η_s	–	74.0	72.8	74.8	86.6	89.5	93.2	100.0[e]
Isentropic efficiency[d]	η_s	–	97.9	95.8	98.4	114.0	115.3	121.9	100.0[e]

[a] Includes chamber compression work and the difference between flow work at discharge and suction ports.
[b] For reference, the isothermal gas compression work is 185.4 kJ kg^{-1}, which is about 72% of that of Case 7 in agreement with Fig. 3.
[c] Calculated adopting equation (12) and the inlet air temperature of Table 4.
[d] Calculated adopting equation (14) and the inlet air temperature of Table 4.
[e] The model accounts only for the irreversibility due to heat transfer between the gas and the liquid phase.

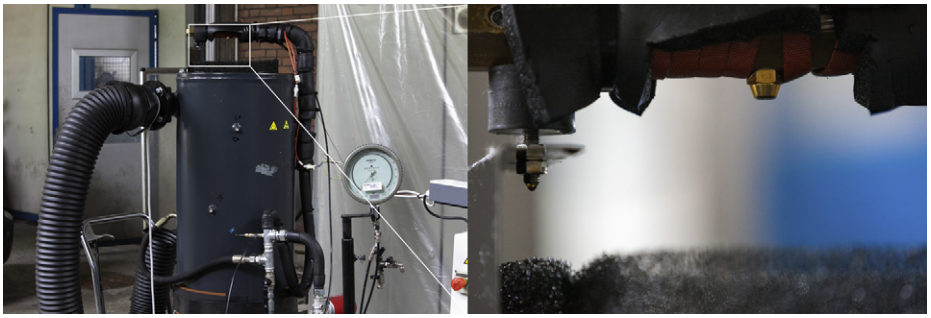

Fig. 6. Photographs of the experimental setup showing, on the left, the bulk oil tank, the nozzle holder, and differential pressure indicator while, on the right, the detail of the nozzle pointing vertically downwards.

compression. All lines are monotonically decreasing starting from relative high values at lower chamber angles because the oil is always hotter than the air. These starting values are definitely higher for gray lines because the oil is heating more effectively the gas at the beginning of the process. However, black lines (that is cases with larger droplets) approach the value of the heat capacity ratio, giving another confirmation that the gas compression is mainly adiabatic; gray lines (smaller droplets) tend to the value of unity, giving another confirmation that the oil is mitigating the gas temperature increase. As expected, Case 7 shows a horizontal line at 1.4.

For each case, Table 5 reports the mass-specific overall work, that includes the chamber compression work and the discharge as well as suction flow works, and the isentropic efficiency, calculated with either equation (12) or equation (14). For reference, the overall work for the isothermal compression (which is the lowest possible) of air from 1 to 9.4 bar is 185.4 kJ kg^{-1}, while that of the gas-only compression (Case 7) is 258.9 kJ kg^{-1}. The isothermal work is about 72% of the gas-only one in agreement with Fig. 3. The cases with coarse droplets (1–3) are characterized by compression works (296.4, 270.5 and 263.3 kJ kg^{-1} respectively) larger than the gas-only case. Fine droplets (cases 4–6) allow instead works that are appreciable smaller (227.1, 224.6 and 212.5 kJ kg^{-1}) than gas-only and permit a valuable energy saving with respect to Case 1 (23.4%, 24.2% and 28.3%). The best compression is Case 6, in which heat transfer from the gas to the liquid is the most effective, with a compression work that is about 82% of that for gas-only compression. However, Fig. 3 shows that the ideal gas–liquid compression is a portion smaller than 82%, which would require an even stronger heat transfer achievable with finer droplets that may be very difficult to generate. Isentropic efficiencies of Case 1 through 3 are in the 72–75% interval. Case 2 with respect to Case 1 has a smaller compression work yet a smaller efficiency simply because the inlet gas temperature is decreased. Decreasing also the inlet liquid temperature (Case 3 with respect to Case 2) up to 2 points can be gained in the efficiency. Decreasing the droplet diameter more than 10 points can be gained. In agreement with Fig. 3, Cases 5 and 6 show that the injection of the optimal amount of liquid, which is later discussed, can lead to improvements of a few points. Computing the isentropic efficiency with equation (14) yields much higher values, even higher than 100%, because the oil presence is completely neglected. It suggests that this second manner of computing the efficiency is misleading because, for instance, the efficiency for a rough compression as that of Case 2 seems to be almost 96%, as if it was close to ideality, whereas it is far from being ideal because the real efficiency is just 73%.

Finally, Fig. 5 shows the mass-specific overall compression work as a function of the liquid-to-gas mass ratio for the Nusselt numbers

Table 6
Description of photographic acquisition system.

Item	Description
Digital camera	
Model	PCO SensicamQE
Sensor size	1280 × 1024 pixels, 6.7 × 6.7 μm^2 square pixel
Lens	
Model	Micro Nikkor F60, F/A ranging from 1.8 to 22, set at 5.6
Image	
Size	58 × 47 mm^2
Resolution	22 pixel mm^{-1}
Pixel size	45.5 μm
Flash	
Model	BINT 850
No. of items	2 flashes
Flash energy	850 mJ each flash
Flash peak duration	6 μs
Peak power	100 kW
Synchronization	
Model	BNC 500C Digital Delay Generator
Resolution	0.1 μs
Repetition	1 Hz

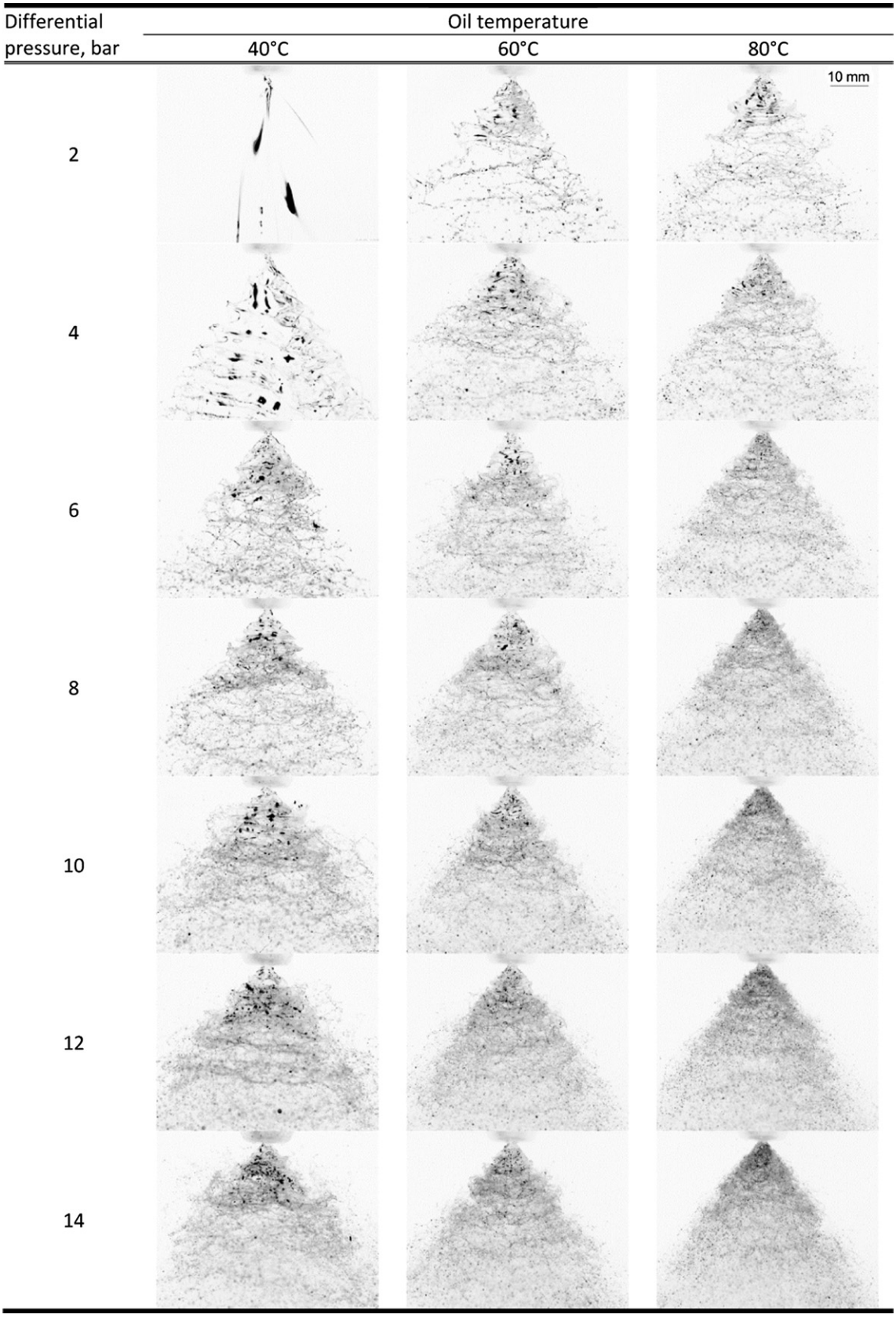

Fig. 7. Evolution of the oil spray at diverse differential pressures and temperatures (images are printed in negative for better visualization). The 10 mm-scale is indicated in the upper-right photo.

of Cases 5 and 6 and all other parameters constant: as suggested by Fig. 3, there is an optimal value for the mass ratio. This optimal value is 16 for Case 5 and 12 for Case 6. If the process was ideal (as in Fig. 3) the optimal would be just 5. As a matter of fact, the better the heat transfer between air and oil, the lower the quantity of oil required to mitigate the gas temperature rise because that quantity is acting effectively.

5. Oil nozzle tests

The necessity to gain more information about the break-up behavior and atomization possibility of the oil suggests an experimental characterization of oil sprays achievable with commercial nozzles. The setup consists of an injection system and a photographic acquisition system with a short-exposure digital camera.

5.1. Test rig

The injection system, pictured in Fig. 6, comprises mainly the nozzle holder, a variable-speed gear pump with the required manometers and regulation valves, and a heating system composed by heating resistances, thermocouples and PID controllers. The oil is injected through the nozzle vertically downwards into a purposely modified oil tank that has the function of both oil reservoir and droplet collector. An external suction system with oil filters is used to keep a slight air flow entering the tank, avoiding the dispersion of the smallest droplets outwards. The spray is generated in an open air ambient in order to skip, at least at this stage, the complexity of a pressurized system.

The photographic acquisition system is of major importance to capture neatly the oil sprays. The system employed the items described accurately in Table 6. The camera is positioned to set the field of view at about few centimeters of width, sufficient to observe the spray development similar to that in the chamber of the mid-size rotary vane compressor here considered. The oil injection differential pressure is expected to be in the order of few bars and, consequently, the Bernoulli formula yields an injection limit velocity in the order of 30 m s^{-1} for a typical oil density. Given the high oil viscosity and the effects of the break-up, the expected droplet velocity should be less than half of the Bernoulli limit, in the order of 10 m s^{-1}, that is 10 μm $μs^{-1}$. The employed acquisition system allows to capture still images because a fast droplet travels in 4 μs less than a pixel size. For comparison, a common camera has an exposure time in the order of 1 ms, during which a droplet could cover up to 10 mm leading to blurred and streaked images; the human eye has an even longer impression time thus visualizing only time-averaged images (see below for an example).

5.2. Experimental evidences

Based on the oil requirement of the mid-size compressor investigated in the heat transfer analysis, the choice for the experimentation falls on a commercial swirl nozzle characterized by a very large nominal flow rate (2.0–2.5 L min^{-1}, that is 30–35 g s^{-1}, for a conventional oil injected at a differential pressure of 10 bar) and by a large nominal angle (80°). The tested injection differential pressures are 2, 4, 6, 8, 10 12 and 14 bar; the oil temperatures 40, 60 and 80 °C. The oil employed in these experiments is a typical lubrication oil characterized by a kinematic viscosity of about 7.5×10^{-5} m^2 s^{-1} at 40 °C and about 1.0×10^{-5} m^2 s^{-1} at 100 °C.

The photos reported in Fig. 7 give evidence of some characteristic behavior of the tested nozzle. All images are printed in negative for better visualization. At the temperature of 40° the oil is still very viscous and, thus, at 2 bar the swirl is nearly not existing leading to the formation of a slightly spread jet with no break-up. At 4 bar a conic film is formed with swirling structures but the break up is not occurring. Starting from 6 bar, break up takes place with the formation of ligaments at 20 mm downstream of the nozzle. Droplets are observed at further distance, with the dimensions of droplets and ligaments decreasing when the injection pressure increases, but the original swirling structures are still clearly visible in the observed field of view. At 60 °C, the conic film is formed already at 2 bar and break-up occurs at all tested pressures at a distance from the nozzle decreasing from 20 to 10 mm at increasing oil pressure. The original swirling structures are still visible, but less than those at 40 °C. Small droplets are visible starting from 6 bar. At 80 °C the break-up is faster, the swirling structures are no more visible starting from 8 bar and small droplets are visible starting from 4 bar.

For comparison, Fig. 8 illustrates average images obtained by superimposing 32 single images, all referring to the same pressure and temperature, for a selected condition. Average images are more similar to what would be obtained by a traditional camera or by the human eye. They are reported to show the difference in the real structure captured in fast exposure images, and thus justify the use of an advanced camera to picture the real phenomenon.

In all cases the images show that the break-up at the tested conditions is not yet complete, which will raise some difficulties in measuring a representative diameter in the next stages of the project. Among the most suitable techniques used to measure the size of droplets, described for instance by Xu [16], diffraction instruments, like a Malvern, or interferometric instruments, like a Phase Doppler Anemometer (PDA), can measure the diameter only of nearly spherical droplets, that in our cases could be only a minor fraction of the oil. Most of the oil appears in the form of ligaments, ramifications or undefined structures. From a heat transfer perspective, ligaments have a large surface with respect to their volume and larger than a sphere having the same volume.

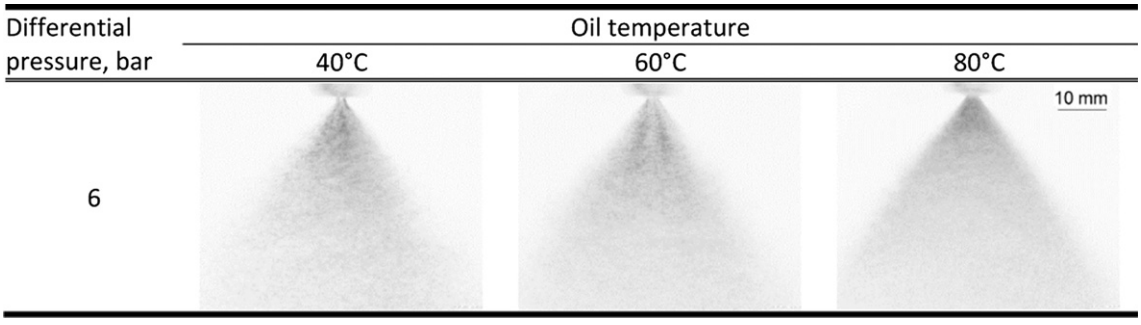

Fig. 8. Average images, obtained by superimposing 32 single images, for a selected condition reported for comparison. Average images are more similar to what would be obtained by a traditional, relatively long exposure camera, or by the human eye (images are printed in negative for better visualization). The 10 mm-scale is indicated in the right photo.

Therefore, despite being different from droplets, they may be effective means for cooling the gas during compression. When exporting experimental results into numerical codes in which the average droplet diameter is considered as a representative parameter, the most appropriate size to represent the liquid ligaments could be their surface mean diameter for heat exchange, or their Sauter mean diameter for the volume to surface ratio [11].

6. Conclusions

The isentropic efficiency of positive-displacement compressors may be improved in order to follow a continuously increasing demand for energy savings. This work analyzes the thermal effect of the oil presence in the gas phase during compression with the scope of exploiting it as a thermal ballast to mitigate both the gas temperature rise and the compression work. The conclusions of the work are listed in the following.

- The energy balance analysis, which considers the overall process from an external viewpoint, shows that a proper amount of liquid (oil) dispersed in a proper manner within a gas (air) can ideally lead to a limited gas temperature increase and a reduced compression work even with respect to 1-time and 2-time intercooled compressions (for working conditions typical of an air compressor).
- The ideal overall compression power (or work) of oil-injected compressors shall be computed with a relation (equation (12)) that comprises the information of the oil presence in order to assess correctly the efficiency of the whole process.
- The heat transfer analysis indicates that the conventional oil injection system leads to oil structures of large dimensions that hinder an effective heat transfer from the gas to the liquid during compression. Reasonably small droplets instead can enhance tremendously the thermal effect of the oil presence.
- Oil droplets of the size of 100 μm permit much lower gas temperatures at the discharge port (as low as 60 °C for a typical rotary vane air compressor) and high energy savings (between 23 and 28% for the same conditions).
- The experimental investigation of a commercial large-flow and large-angle oil nozzle confirms that at the operating temperature of the compressor, break-up occurs starting from a low differential pressure generating small droplets as well as ligaments, ramifications and undefined structures.
- From an heat transfer perspective ligaments, ramifications and undefined structures have a large exchange surface with respect to their volume, allowing for a very effective heat exchange, but may generate difficulties when attempting to measure the droplet diameters or their equivalent diameters.
- This work is in agreement with almost all the reviewed publications from the open literature which conclude that oil distribution, quantity and temperature have an important thermal effect that can be exploited for improving the performance of oil-injected compressors of any type.

In the next stage of the project, other nozzles from the market or specifically-designed ones will be investigated with the setup here described. The most suitable will be mounted on the mid-size compressor considered in this work for the experimental proof of the concepts here exposed.

Acknowledgements

The authors are sincerely grateful to Ing Enea Mattei S.p.A. and, in particular, to Dr. Giulio Contaldi, CEO, for the theoretical and material support offered during the study.

Nomenclature

Acronyms

PDA	Phase Doppler Anemometer
rpm	revolutions per minute

Symbols

$\widehat{\Theta}$	modified gas theta parameter [−]
Ω	rotational speed of the shaft [rpm]
α	heat transfer coefficient at the droplet surface [W m^{-2} K^{-1}]
ε	liquid-to-gas ratio [−]
ϑ	chamber angle [°]
λ	ratio of the temperature increase of an ideal compression with respect to the ideal gas-only (adiabatic) compression [−]
ρ	density [kg m^{-3}]
τ	ratio of the compression power of an ideal compression with respect to the ideal gas-only (adiabatic) compression [−]
A	heat transfer area of the oil droplets [m^2]
Bi	Biot number [−]
D	droplet diameter [m]
$\dot{L}$	compression power taken positive if transfer to the system [W]
M	molar mass [kg kmol^{-1}]
N	number of droplets
$\mathrm{Nu_D}$	Nusselt number [−]
P	pressure [Pa]
Pr	Prandtl number [−]
Q	heat between gas and liquid [J]
R	gas constant [J kg^{-1} K^{-1}]
$\mathrm{Ra_D}$	Rayleigh number [−]
$\mathrm{Re_D}$	Reynolds number [−]
$\dot{S}_{\mathrm{irr}}$	rate of entropy generation [W K^{-1}]
T	temperature [K]
U	internal energy [J]
V	volume [m^3]
c	mass specific heat [J kg^{-1} K^{-1}]
$\widehat{c}$	modified mass specific heat [J kg^{-1} K^{-1}]
k	thermal conductivity [W m^{-1} K^{-1}]
h	mass-specific enthalpy [J kg^{-1}]
j	number of intercooled compression stages
l	mass-specific overall compression work taken positive if transferred to the system [J kg^{-1}]
l^{g}	mass-specific chamber compression work taken positive if transferred to the system [J kg^{-1}]
m	mass [kg]
$\dot{m}$	mass flow [kg s^{-1}]
n	equivalent compression index [−]
s	mass-specific entropy [J kg^{-1} K^{-1}]
t	time [s]

Superscripts

g	gas
l	liquid

Subscripts

c	specific heat
f	final
i	initial
m	mass
p	at constant pressure

s at constant entropy
v at constant volume
x along a generic compression process

References

[1] S. Bracco, A. Pierfederici, A. Trucco, The wet compression technology for gas turbine power plants: thermodynamic model, Applied Thermal Engineering 27 (4) (2007) 699–704.
[2] C.A. Infante Ferreira, C. Zamfirescu, D. Zaytsev, Twin screw oil-free wet compressor for compression–absorption cycle, International Journal of Refrigeration 29 (4) (2006) 556–565.
[3] P.J. Singh, J.L. Bowman, Heat transfer in oil-flooded screw compressors, in: Proc. International Compressor Engineering Conference at Purdue, Lafayette, IN, USA, 1986, pp. 135–152.
[4] N. Stosic, A. Kovacevic, K. Hanjalic, L. Milutinovic, Mathematical modelling of the oil influence upon the working cycle of screw compressors, in: Proc. International Compressor Engineering Conference at Purdue, Lafayette, IN, USA, 1988, pp. 354–361.
[5] N. Stosic, L. Milutinovic, K. Hanjalic, A. Kovacevic, Investigation of the influence of oil injection upon the screw compressor working process, International Journal of Refrigeration 15 (4) (1992) 206–220.
[6] M. Fujiwara, Y. Osada, Performance analysis of an oil-injected screw compressor and its application, International Journal of Refrigeration 18 (4) (1995) 220–227.
[7] M. De Paepe, D. Mertens, W. Bogaert, Cooling of oil injected screw compressors by oil atomisation, Applied Thermal Engineering 25 (17–18) (2005) 2764–2779.
[8] N. Seshaiah, S.K. Ghosh, R.K. Sahoo, S.K. Sarangi, Mathematical modeling of the working cycle of oil injected rotary twin screw compressor, Applied Thermal Engineering 27 (1) (2007) 145–155.
[9] N. Seshaiah, R.K. Sahoo, S.K. Sarangi, Theoretical and experimental studies on oil injected twin-screw air compressor when compressing different light and heavy gases, Applied Thermal Engineering 30 (4) (2010) 327–339.
[10] R. Cipollone, G. Contaldi, A. Capoferri, R. Valente, Theoretical and experimental study of the $p-V$ diagram for a sliding vane rotary compressor, in: IMechE International Conference on Compressors and Their Systems, London, UK 2009, pp. 279–289.
[11] A.H. Lefebvre, Atomization and Sprays, Hemisphere Publishing Corporation, New York, NY, USA, 1989.
[12] F.P. Incropera, D.P. DeWitt, Introduction to Heat Transfer, John Wiley & Sons, New York, NY, USA, 1996.
[13] W. Ranz, W. Marshall, Evaporation from droplets, part II, Chemical Engineering Progress 48 (1952) 141–146.
[14] S.W. Churchill, Free Convection Around Immersed Bodies, in: G.F. Hewitt (Ed.), Heat Exchanger Design Handbook, Begell House, New York, NY, USA, 2002.
[15] A. Quarteroni, R. Sacco, F. Saleri, Numerical Mathematics, Springer-Verlag, New York, NY, USA, 2000.
[16] R. Xu, Particle Characterization: Light Scattering Methods, Kluwer Academic Publishers, Dordrecht, The Netherlands, 2000.